



**HAL**  
open science

## Comparison of perfused volume segmentation between cone-beam CT and $^{99m}\text{Tc}$ -MAA SPECT/CT for treatment dosimetry before selective internal radiation therapy using $^{90}\text{Y}$ -glass microspheres

M. Martin, A. Hocquelet, F. Debordeaux, L. Bordenave, J.-F. Blanc, P. Papadopoulos, B. Lapuyade, H. Trillaud, J.-B. Pinaquy

### ► To cite this version:

M. Martin, A. Hocquelet, F. Debordeaux, L. Bordenave, J.-F. Blanc, et al.. Comparison of perfused volume segmentation between cone-beam CT and  $^{99m}\text{Tc}$ -MAA SPECT/CT for treatment dosimetry before selective internal radiation therapy using  $^{90}\text{Y}$ -glass microspheres. *Diagnostic and Interventional Imaging*, 2021, 102, pp.45 - 52. 10.1016/j.diii.2020.09.003 . hal-03493594

**HAL Id: hal-03493594**

**<https://hal.science/hal-03493594>**

Submitted on 2 Jan 2023

**HAL** is a multi-disciplinary open access archive for the deposit and dissemination of scientific research documents, whether they are published or not. The documents may come from teaching and research institutions in France or abroad, or from public or private research centers.

L'archive ouverte pluridisciplinaire **HAL**, est destinée au dépôt et à la diffusion de documents scientifiques de niveau recherche, publiés ou non, émanant des établissements d'enseignement et de recherche français ou étrangers, des laboratoires publics ou privés.



Distributed under a Creative Commons Attribution - NonCommercial 4.0 International License

# Comparison of perfused volume segmentation between cone-beam CT and $^{99m}\text{Tc}$ -MAA SPECT/CT for treatment dosimetry before selective internal radiation therapy using $^{90}\text{Y}$ -glass microspheres

Short title

## Cone-beam CT for pre-treatment dosimetry before SIRT

M. Martin <sup>a,\*</sup>, A. Hocquelet <sup>b</sup>, F. Debordeaux <sup>a</sup>, L. Bordenave <sup>a,c</sup>, J.-F. Blanc <sup>d</sup>, P. Papadopoulos <sup>a</sup>, B. Lapuyade <sup>a</sup>, H. Trillaud, MD <sup>a,e</sup>, J.-B. Pinaquy <sup>a</sup>

<sup>a</sup> Department of Radiology, CHU Bordeaux, CIC1401, 33000 Bordeaux, France

<sup>b</sup> Department of Radiology, CHU Vaudois, 1011, Lausanne, Switzerland.

<sup>c</sup> Univ. Bordeaux, INSERM, Bioingénierie tissulaire, U1026, 33000 Bordeaux, France.

<sup>d</sup> Department of Gastroenterology-Hepatology, Hôpital Haut-Lévêque, CHU Bordeaux, 33000 Bordeaux, France.

<sup>e</sup> Univ. Bordeaux, Institut de mathématique, MONC, UMR 5251, 33000 Bordeaux, France.

\* Corresponding author: [manuel.hr.martin@gmail.com](mailto:manuel.hr.martin@gmail.com)

## Abstract

**Purpose:** To compare the reliability and accuracy of the pre-treatment dosimetry predictions using cone-beam computed tomography (CBCT) versus <sup>99m</sup>Tc-labeled macroaggregated albumin (MAA) SPECT/CT for perfused volume segmentation in patients with hepatocellular carcinoma treated by selective internal radiation therapy (SIRT) using <sup>90</sup>Y-glass microspheres.

**Materials and methods:** Fifteen patients (8 men, 7 women) with a mean age of  $68.3 \pm 10.5$  (SD) years (range: 47–82 years) who underwent a total of 17 SIRT procedures using <sup>90</sup>Y-glass microspheres for unresectable hepatocellular carcinoma were retrospectively included. Pre-treatment dosimetry data were calculated from <sup>99m</sup>Tc-MAA SPECT/CT using either CBCT or <sup>99m</sup>Tc-MAA SPECT/CT to segment the perfused volumes. Post-treatment dosimetry data were calculated using <sup>90</sup>Y imaging (SPECT/CT or PET/CT). The whole liver, non-tumoral liver, and tumor volumes were segmented on CT or MRI data. The mean absorbed doses of the tumor (DT), non-tumoral liver, perfused liver (DPL) and perfused non-tumoral liver were calculated. Intra- and interobserver reliabilities were investigated by calculating Lin's concordant correlation coefficients ( $\rho_c$  values). The differences (biases) between pre- and post-treatment dosimetry data were assessed using the modified Bland–Altman method (for non-normally distributed variables), and systematic bias was evaluated using Passing–Bablok regression.

**Results:** The intra- and interobserver reliabilities were good-to-excellent ( $\rho_c$ : 0.80 – 0.99) for all measures using both methods. Compared with <sup>90</sup>Y imaging, the median differences were 5.8 Gy (IQR: -12.7; 16.1) and 5.6 Gy (IQR: -13.6; 10.2) for DPL-CBCT and DPL-<sup>99m</sup>Tc-MAA SPECT/CT, respectively. The median differences were 1.6 Gy (IQR: -29; 7.53) and 9.8 Gy (IQR: -28.4; 19.9) for DT -CBCT and DT -<sup>99m</sup>Tc-MAA SPECT/CT respectively. Passing–Bablok regression analysis showed that both CBCT and <sup>99m</sup>Tc-MAA SPECT/CT had proportional biases and thus tendencies to overestimate DT and DPL at higher post-treatment doses.

**Conclusion:** CBCT may be a reliable segmentation method, but it does not significantly increase the accuracy of dose prediction compared with that of <sup>99m</sup>Tc-MAA SPECT/CT. At higher doses both methods tend to overestimate the doses to tumors and perfused livers.

Keywords: Brachytherapy; Radiation Dosimetry; Yttrium-90; Carcinoma, hepatocellular; Cone-beam CT; SPECT CT

## **Abbreviations**

<sup>90</sup>Y, Yttrium-90;

95% CI, 95% confidence interval;

<sup>99m</sup>Tc, Technetium-99m;

BCLC, Barcelona Clinic Liver Cancer;

CBCT, Cone-Beam computed tomography;

CD-CTHA, Catheter-directed computed tomography hepatic angiography;

CT, Computed tomography;

ICC, Intraclass coefficient correlation;

HCC, Hepatocellular carcinoma;

MAA, Macroaggregated albumin;

MELD, Model for End-stage Liver Disease;

MIRD, Medical internal radiation dose;

MRI, Magnetic resonance imaging;

PET, Positron emission tomography;

Q1, First quartile;

Q3, Third quartile;

SIRT, Selective internal radiation therapy;

SPECT/CT, Single-photon emission computed tomography/computed tomography;

SD, Standard deviation;

T/N, Tumor-to-normal tissue ratio;

VOI, Volume-of-interest.

## Introduction

Selective internal radiation therapy (SIRT), also referred to as radioembolization or transarterial radioembolization, is aimed at delivering the optimal radiation dose to tumor, related to treatment goal, while sparing the non-tumoral liver tissue (especially in cirrhotic patients). Recently, dosimetry considerations of SIRT have evolved markedly, given the development of personalized pre-treatment dosimetry based on  $^{99m}\text{Tc}$ -labeled macroaggregated albumin (MAA) single-photon emission/computed tomography (SPECT/CT). This provides important information such as tumor-to-normal tissue ratio (T/N) and perfused-to-total hepatic volume ratio [1]. This multi-compartmental method enables good prediction of post-treatment dosimetry data [2, 3]. Moreover the threshold tumor dose of 205 Gy is highly predictive of response and overall survival for glass microspheres [4]. However, the technique is very sensitive to segmentation of tumor and perfused volume.

No consensus on the optimal pre-treatment dosimetry method has yet emerged. Accurate evaluation of the target liver volume is fundamental; this directly affects the absorbed dose estimation. The perfused volume is delimited using various techniques (such as adaptive thresholding) based on the liver boundaries evident on SPECT/CT images, or using anatomical landmarks and co-registration of baseline images [5] or thresholding of the maximum activity [3]. A less common method, proposed by Kao et al., uses targeted arterial territories identified via catheter-directed CT hepatic angiography for delineation of the volume of interest (VOI) on  $^{99m}\text{Tc}$ -MAA SPECT/CT [6]. This facilitates use of a patient-specific, arterial volume-based approach regardless of any variation in vascular anatomy, tissue distortion by the tumor, or previous treatments. Per-procedure C-arm CBCT is now used routinely during SIRT work-up (simulation) to map the vascular anatomy and liver tissue perfusion, allowing selection of the optimal catheter position [7-9]. CBCT may afford a better estimation of perfused volume and more reliable segmentation compared with  $^{99m}\text{Tc}$ -MAA SPECT/CT alone or with the use of anatomical landmarks [10-12].

The purpose of this study was to compare the reliabilities and accuracies of pre-treatment dose predictions of CBCT and  $^{99m}\text{Tc}$ -MAA SPECT/CT in terms of perfused volume segmentation in patients with unresectable hepatocellular carcinoma (HCC) treated by SIRT using  $^{90}\text{Y}$ -glass microspheres.

## Materials and methods

### *Patient selection*

We retrospectively analyzed the data of patients treated with SIRT using  $^{90}\text{Y}$ -glass microspheres (TheraSphere®) as prescribed by our institution's multidisciplinary liver tumor board, from December 2014 to June 2019 at the University Hospital of Bordeaux, France. Informed consent was obtained from all individual participants included in this study. The inclusion criteria were unresectable HCC treated with only a single  $^{90}\text{Y}$ -glass microsphere injection at the same injection site used for  $^{99\text{m}}\text{Tc}$ -MAA SPECT/CT.

Twenty patients with such treatments were identified during the study period, but five were excluded from the analysis for the following reasons: the injection sites for planning and treatment angiography differed significantly (n=1), multiple injection sites (n=3), and low-quality (artifact-containing)  $^{99\text{m}}\text{Tc}$ -MAA SPECT/CT data (n=1).

The study population included 15 patients (8 men, 7 women) with a mean age of  $68.3 \pm 10.5$  (SD) years (range: 47–82 years) who underwent SIRT procedures using  $^{90}\text{Y}$ -glass microspheres for unresectable HCC. All patients received microsphere injections in a single session. Two patients underwent two SIRT procedures that were considered as distinct procedures; thus, the study included 17 SIRT procedures. Figure 1 shows the study flow chart.

### *General procedure*

The SIRT procedure has been described in detail elsewhere [13–16]. Briefly, all patients underwent baseline, multiphase, contrast-enhanced magnetic resonance imaging (MRI) or CT of the liver within 1 month before planning angiography. The work-up was performed using digital subtraction angiography and contrast-enhanced CBCT. CBCT acquisition was performed with a C-arm rotation (Artis® Zee, Siemens Healthineers) that covered a range of  $199^\circ$  ( $0.5^\circ/\text{image}$ ), with  $30 \times 40 \text{ cm}^2$  flat-panel detector with a reconstructed volume of  $24 \times 24 \times 18 \text{ cm}^3$ . The latter was performed with a single injection of contrast agent and one acquisition with a delay of 10 s and full rotation of 6 s. A selective catheterization with a microcatheter (Direxion® 2.4-F Boston Scientific or Progreat® 2.7-F Terumo) was performed in all procedures. In general, the microcatheter was positioned at the right or left main branch of the hepatic artery while, rarely a more selective position was obtained at the level of a sectorial or segmental branch. The injection rate was selected to obtain optimal

opacification while avoiding reflux of contrast material in non-target arteries. The injection rate ranged from 0.5 mL/s for selective opacification to 1 mL/s for less selective ones. This acquisition protocol enabled simultaneous evaluation of tumor vascular supply, tumor enhancement, and liver tissue perfusion. An automatic feeder detection software (Syngo® Embolization guidance) was used when needed [17]. At the end of mapping angiography, approximately 167 MBq  $^{99m}\text{Tc}$ -MAA were injected into the target artery, and planar images were acquired for assessment of lung shunt fraction. Hepatic SPECT/CT was used to identify potential extrahepatic deposition, plan tumor targeting and calculate pre-treatment dosimetry data. The activity to be delivered was calculated as follows: (i), for the first 11 procedures, using a mono-compartment model based on the medical internal radiation dose (MIRD) formalism with an absorbed dose of 80 – 150 Gy to the perfused liver based on the instructions for use [18], or (ii), for the last 6 procedures, via a personalized multi-compartment model using dedicated software (Simplicit $^{90}\text{Y}$ <sup>TM</sup>). Glass  $^{90}\text{Y}$  microspheres were injected after a median delay of 9 days (IQR: 8; 15 days) after simulation, followed by  $^{90}\text{Y}$  imaging using SPECT/CT (11 procedures) or PET/CT (6 procedures) to assess the biodistributions of the  $^{90}\text{Y}$  microspheres and calculate post-treatment dosimetry data. All  $^{90}\text{Y}$  images were acquired the following day (between 20 and 24h) after the injection of  $^{90}\text{Y}$  microspheres.

### *Dosimetry evaluation*

Dedicated software (Simplicit $^{90}\text{Y}$ <sup>TM</sup>) was used to build personalized multi-compartment models using three-dimensional dosimetry data at a voxel level. The first step was rigid co-registration of the baseline images derived using CBCT,  $^{99m}\text{Tc}$ -MAA SPECT/CT and  $^{90}\text{Y}$  imaging (PET/CT or SPECT/CT) with manual adjustment when needed. The second step featured manual segmentation of the VOIs using baseline MRI (n = 4) or CT (n = 13) examination to define total liver volume and tumor volume. Only lesions > 2 cm in diameter lying in the perfused volume were delineated, to minimize any bias due to partial-volume effect. The non-tumoral liver volume was obtained for toxicity assessment by subtracting the tumor volume from the total liver volume. The perfused liver volume ( $V_{\text{PL}}$ ) was the targeted hepatic volume (depending on the specific artery) delineated using CBCT or  $^{99m}\text{Tc}$ -MAA SPECT/CT pre-treatment and  $^{90}\text{Y}$  imaging post-treatment. In terms of pre-treatment CBCT dosimetry, co-registration of the CBCT and  $^{99m}\text{Tc}$ -MAA SPECT/CT images enabled artery-specific tissue volume delineation and yielded the corresponding T/N. The non-tumoral

volume within the  $V_{PL}$  was calculated automatically by subtracting the tumor volume from  $V_{PL}$ . The  $V_{PL}$  was drawn manually for CBCT; contours were defined on every third to fifth liver slice. The software then extrapolated the entire perfused volume. For two patients, the outermost portion of the perfused volume was not contained in the acquisition field-of-view of CBCT and was extrapolated by co-registration to the edges of the liver. If necessary, co-registration of the (CBCT-revealed) perfused volume to the baseline image was adjusted to ensure that the edges of the perfused volume matched the limits of the liver.  $V_{PL}$  was semi-automatically defined for  $^{99m}\text{Tc}$ -MAA SPECT/CT; segmentation afforded both activity and volume data based on thresholding. The volumes and total counts were provided for each VOI (perfused liver, tumor, and perfused non-tumoral liver). The threshold value selected (% maximum activity) incorporated all VOI voxels that met the criterion. The threshold value was adjusted to make the edges of the perfused volumes match the limits of the liver seen on the fused images (Fig. 2). The  $^{99m}\text{Tc}$ -MAA SPECT/CT segmentation method was used for  $^{90}\text{Y}$  imaging. When using  $^{90}\text{Y}$  PET for post treatment dosimetry, a direct microspheres quantification was obtained, measuring radioactivity (Bq/ml) for each VOI. For each treatment session, the mean doses absorbed by the tumor ( $D_T$ ), non-tumoral liver ( $D_{NLT}$ ), perfused liver ( $D_{PL}$ ), and perfused non-tumoral liver ( $D_{PNLT}$ ) were calculated using VOI from CBCT,  $^{99m}\text{Tc}$ -MAA SPECT/CT, and  $^{90}\text{Y}$  imaging. The software then calculated the mean absorbed dose for each VOI based on these activities. The early version of the program yielded only isodose curves, not dose–volume histograms. When calculating the absorbed doses, the software used the MIRD formalism to directly translate activity in Bq to an absorbed dose in Gy. Voxel-based doses were calculated employing a local deposition method.

### *Primary and secondary outcomes*

The primary outcomes were the dose prediction accuracies of CBCT and  $^{99m}\text{Tc}$ -MAA SPECT/CT in terms of the mean absorbed doses in each compartment, with the  $^{90}\text{Y}$  imaging data serving as the reference. The secondary outcomes were intra- and interobserver reliabilities in dose predictions and perfused volumes (for both CBCT and  $^{99m}\text{Tc}$ -MAA SPECT/CT). All dosimetry evaluation steps were performed twice by the first reviewer (M.M, a junior radiologist with 3 years of experience) and once by the second reviewer (J-B.P, a nuclear medicine physician specializing in SIRT with 10 years of experience); both



reviewers were mutually blinded to each other's results. Absorbed doses were expressed in Gy, activities in GBq, and perfused volumes in cm<sup>3</sup>.

### *Statistical analysis*

Statistical analyses were performed using STAT software (StatCorp®). Quantitative variables were expressed as means  $\pm$  standard deviations (SDs) and ranges for normally distributed variables and as medians and interquartile ranges (IQR) otherwise. Qualitative variables were expressed as raw numbers, proportions and percentages. Data distribution was assessed using the Shapiro–Wilk test. Lin's concordance correlation coefficients ( $\rho_c$  values) was used to assess intra- and interobserver reliabilities [19], which is similar to the intraclass coefficient correlation but more appropriate for not normally distributed variables.  $\rho_c$  values were classified as  $< 0.50$ , unacceptable;  $0.51 - 0.60$ , poor;  $0.61 - 0.70$ , mediocre;  $0.71 - 0.80$ , satisfactory;  $0.81 - 0.90$ , fairly good;  $0.91 - 0.95$ , very good; and  $> 0.95$  excellent [20]. Pre- and post-treatment dosimetry data were compared using Bland–Altman analysis of the differences in the median predicted and actual doses. Medians along with IQRs were used because the data were not normally distributed [21]. Systematic bias was searched for using Passing–Bablok regression. Results were presented as scatter diagrams with regression lines. Each regression equation ( $y = a + bx$ ) included a constant (the intercept  $a$ ) and a proportional difference (the slope  $b$ ). The 95% confidence intervals (95% CIs), which reveal whether the slope differed from 1 only by chance, were also reported. If 95% CI for slope ( $b$ ) included value 1, it cannot be concluded that there is a proportional difference between two methods [22,23].

## **Results**

### *Patients details and procedures characteristics*

Procedures characteristics are summarized in Table 1. Sixteen procedures (16/17; 94%) involved patients with advanced disease and one intermediate stage (1/17; 6%) according to the BCLC (Barcelona Clinic Liver Cancer) staging system, usually with portal vein thrombosis (15/17; 88%) but preserved liver function (Child–Pugh status  $\leq$  B7). The mean MELD (Model for End-Stage Liver Disease) score was  $8.7 \pm 1.8$  (SD) (range: 6 – 12) [24]. Twelve procedures (12/17; 71%) were hemiliver treatment, 4 (4/17; 23%) sectorial, and 1 (1/17; 6%) segmental. The mean radioactivity administered was 1.91 GBq (range: 0.23–4.43

GBq). The median  $D_T$  values were 198.3 Gy (IQR: 150.3; 306.2) for CBCT, 187.2 (IQR: 148.2; 296.7) Gy for  $^{99m}\text{Tc}$ -MAA SPECT/CT, and 200.6 (IQR: 138.1; 268.2) Gy for  $^{90}\text{Y}$  imaging. The median  $D_{\text{NTL}}$  (values were 41.9 Gy (IQR: 15.3; 55.5) for CBCT, 45.8 Gy (IQR: 26.7; 57.1) for  $^{99m}\text{Tc}$ -MAA SPECT/CT, and 46.3 Gy (IQR: 35.4; 58) for  $^{90}\text{Y}$  imaging (Fig. 3).

### *Comparison of pre- and post-treatment dosimetry data*

The pre- and post-treatment dosimetry data are reported in Table 2. The  $D_T$  and  $D_{\text{NTL}}$  pre- and post-treatment dosimetry data obtained using CBCT and  $^{99m}\text{Tc}$ -MAA SPECT/CT are displayed in Fig. 4. By comparison with the  $^{90}\text{Y}$  imaging data, the median differences were 5.8 Gy (IQR: -12.7; 16.1) and 5.6 Gy (IQR: -13.6; 10.2) for  $D_{\text{PL}}$ -CBCT and  $D_{\text{PL}}$ - $^{99m}\text{Tc}$ -MAA SPECT/CT, respectively. The median differences were 1.6 Gy (IQR: -29; 7.53) and 9.8 Gy (IQR: -28.4; 19.9) for  $D_T$ -CBCT and  $D_T$ - $^{99m}\text{Tc}$ -MAA SPECT/CT, respectively. At Passing–Bablok regression analysis CBCT and  $^{99m}\text{Tc}$ -MAA SPECT/CT proportionally overestimated the predicted doses delivered to tumors and perfused livers.

The Passing-Bablok regression equations were as follows:  $y = 56.65 + 0.66 x$  (95% CI  $b = 0.55 - 0.90$ ) for  $D_{\text{PL}}$ -CBCT,  $y = 35.30 + 0.77 x$  (95% CI  $b = 0.56 - 0.96$ ) for  $D_{\text{PL}}$ - $^{99m}\text{Tc}$ -MAA SPECT/CT,  $y = 43.11 + 0.75 x$  (95% CI  $b = 0.61 - 0.94$ ) for  $D_T$ -CBCT, and  $y = 40.35 + 0.77x$  (95% CI  $b = 0.62 - 1.03$ ) for  $D_T$ - $^{99m}\text{Tc}$ -MAA SPECT/CT (Fig.5). Thus, the higher the dose, the greater the risk of overestimation. No systematic dose prediction biases were found for either non-tumoral or perfused non-tumoral livers. Concerning all procedures realized, there was none where a predicted tumoricidal  $^{99m}\text{Tc}$ -MAA SPECT/CT dose ( $> 205$  Gy) was not confirmed with post-treatment dosimetry data. On the other hand, for one procedure the pre-treatment tumoricidal dose ( $D_T$ ) predicted by CBCT was 220 Gy, and the post-treatment  $D_T$  was 200.6 Gy. The difference was within our margin of error (median: 1.56 Gy; IQR: -29; 7.53). Finally, for one procedure (procedure number 15), neither CBCT ( $D_T = 198.3$  Gy) nor  $^{99m}\text{Tc}$ -MAA SPECT/CT ( $D_T = 200.1$  Gy) predicted the same tumoricidal dose indicated by  $^{90}\text{Y}$  imaging ( $D_T = 248.1$  Gy) (Table 3).

In one of our patients, CBCT was more accurate than  $^{99m}\text{Tc}$ -MAA SPECT/CT (Fig. 6). Segment IV perfusion was not apparent on  $^{99m}\text{Tc}$ -MAA SPECT/CT, but the segment was well-perfused on CBCT and  $^{90}\text{Y}$  imaging. A preferential flow phenomenon may develop if injection is inappropriate. Intra-arterial injection of  $^{99m}\text{Tc}$ -MAA must be slow (60 s), mirroring injection of the  $^{90}\text{Y}$  microspheres.

### *Intra- and interobserver reliabilities*

The data are summarized in Table 4. Excellent, very good, or fairly good agreements were found for all variables except for  $D_{\text{PNTL}}$  interobserver reliability using  $^{99\text{m}}\text{Tc}$ -MAA SPECT/CT ( $\rho_c = 0.80$ ).

## **Discussion**

Reliable pre-treatment dosimetry planning requires accurate input dosimetry parameters so that tissue masses and count ratios are critical in this context. Hemiliver or segmental SIRT, which has become increasingly common, requires accurate volumetric measurements within the targeted arterial territories [25]. Although CBCT is now integrated with SIRT, any dosimetry role for CBCT remains unclear. O'Connor et al. found that hemiliver and tumor volumes measured using CBCT were as reliable as baseline MRI data and could be used for dose calculations employing the MIRD mono-compartment model of glass microspheres [10]. This study is the first to investigate whether perfused volume segmentation using CBCT allows an individualized dosimetry approach using  $^{90}\text{Y}$ -glass microspheres, similar to segmentation employing  $^{99\text{m}}\text{Tc}$ -MAA SPECT/CT.

Overall, good correlation was evident between the pre-treatment dosimetry data (derived using CBCT or  $^{99\text{m}}\text{Tc}$ -MAA SPECT/CT) and post-treatment data. For  $D_{\text{T}}$ , the median differences were 1.6 Gy (IQR: -29; 7.53) Gy and 9.8 Gy (IQR: -28.4; 19.9) between  $^{90}\text{Y}$  imaging, and CBCT and  $^{99\text{m}}\text{Tc}$ -MAA SPECT/CT, respectively. For  $D_{\text{PL}}$ , the median differences were 5.8 Gy (IQR: -12.7; 16.1) and 5.6 Gy (IQR: -13.6; 10.2) between  $^{90}\text{Y}$ -imaging and CBCT or  $^{99\text{m}}\text{Tc}$ -MAA SPECT/CT respectively. From a clinical perspective, there was no difference in mean absorbed doses calculated between the two pre-treatment methods, except for the  $D_{\text{PNTL}}$  for which  $^{99\text{m}}\text{Tc}$ -MAA SPECT/CT was more accurate. These results should be considered particularly when SIRT is used to induce contralateral hypertrophy. Recently, Palart et al. found an association between  $D_{\text{NTL}}$  and contralateral liver hypertrophy; the  $D_{\text{NTL}}$  threshold was  $\geq 88$  Gy when the maximal hypertrophy of the untreated lobe was  $\geq 10\%$  [26]. It is particularly difficult to define a SIRT toxicity threshold, as there are many confounding factors such as definition of toxicity, hepatic reserve, underlying liver disease, and treated volume [27]. In our study, differences in the pre- and post-treatment  $D_{\text{NTL}}$  using both  $^{99\text{m}}\text{Tc}$ -MAA SPECT/CT (median: 0.57 Gy; IQR: -1.9; 8.9) and CBCT (median: 2.5; IQR: -1.5; 11.7) were very low and therefore not clinically relevant. Thus, CBCT

segmentation of the perfused liver yields safe and accurate pre-treatment dosimetry predictions.

We found some systematic biases in dose evaluation to the perfused liver and tumor; higher predicted doses tended to be overestimated, and the threshold was approximately 300 – 350 Gy. From a radiobiological viewpoint, this must be kept in mind, as SIRT success requires delivery of a tumoricidal dose. The more this is exceeded, the greater the effect, up to a maximum. Note that this was only a trend when  $D_T$  was calculated using  $^{99m}\text{Tc}$ -MAA SPECT/CT using Passing–Bablok regression. A recent study on glass microspheres found good correlations between  $^{99m}\text{Tc}$ -MAA SPECT/CT and post-treatment dosimetry, with no systematic over- or underestimation. No  $D_T$  value exceeded 300 Gy, which could explain the absence of systematic bias [2]. Jadoul et al. found that variations between pre- and post-treatment dosimetry data were markedly higher for tumors than for non-tumoral livers, especially for tumors exhibiting major uptake, but they did not statistically evaluate systematic bias [3].

We sought to standardize pre-treatment dosimetry segmentation using CBCT, as no standard pre-treatment dosimetry method has been established yet. The use of baseline imaging only (with anatomical landmarks) to delineate the perfused volume is well accepted in some scenarios, including radiation segmentectomy or lobectomy [28]. However, the T/N ratio obtained via  $^{99m}\text{Tc}$ -MAA SPECT/CT and voxel-based dosimetry are often essential for dose predictions. Either anatomical or functional imaging, or both, may be used [29]. None of these methods is perfect, and all are associated with possible errors.

In our study, both CBCT and  $^{99m}\text{Tc}$ -MAA SPECT/CT were reproducible and reliable, with neither being superior to the other. Intra- and interobserver reliabilities in terms of  $D_T$  and  $D_{PL}$  calculations were very good to excellent ( $\rho_c$ : 0.95 – 0.99) for both methods; this is important given the number of steps involved in the evaluation.

For tumors supplied by multiple arteries, several dosimetry method options exist, and no single method is superior. This was evaluated by Ray et al. from the perspective of  $^{90}\text{Y}$ -microsphere distribution [30]. Given the developments in personalized predictive dosimetry, such a situation is challenging during work-up. A single work-up might result in overlap of the perfused volumes after two or more injections of  $^{99m}\text{Tc}$ -MAA, rendering it impossible to calculate the precise activity required in each location. However, multiple sessions are associated with organizational problems and delays. Thus, the CBCT perfused volume may be

particularly useful during work-up prior to multiple injections. As described by Kao et al., integration of the perfused catheter-directed CT hepatic angiography or CBCT volumes in the planned dosimetry for each catheter position should allow accurate dose calculations for all catheters; thus, a single work-up session may be sufficient [6].

Our study has several limitations. First, this was a retrospective, single-center study with a small number of patients. Caution should be advised when extrapolating the results as our study population included only patients with HCC treated with glass microspheres. We delineated the entire tumor without excluding nonviable regions. During scan co-registration, some radioactivity may be excluded from the VOI. This is an inherent weakness of multi-modal imaging co-registration. However, this had limited impact on our work, as we were concerned with VOIs, not voxels. A related limitation is the use of rigid, rather than deformable registration. However, the use of a non-rigid registration was beyond the scope of this study and should be investigated in future work. The use of two post-treatment dosimetry modalities ( $^{90}\text{Y}$  PET/CT and  $^{90}\text{Y}$  SPECT/CT) remains debatable. PET affords better spatial resolution and quantification accuracy than does SPECT, especially in smaller lesions [31,32]. Therefore, we considered only lesions larger than 2 cm and it is possible to derive reasonably accurate activity estimates from bremsstrahlung SPECT images if appropriate compensations are applied during reconstruction [33,34]. Regarding CBCT, several limitations are intrinsic to this technique, including a limited field of view, artifacts, and the need for patients to assume certain positions and hold their breath [7]. As  $^{99\text{m}}\text{Tc}$ -MAA, contrast agent molecules have different physical properties (size, density) and the injection volume and velocity differ from those of microspheres. Thus, microsphere and contrast agent distributions may or may not be identical. Pre-treatment CBCT dosimetry is closely related to  $^{99\text{m}}\text{Tc}$ -MAA SPECT/CT for T/N counts; currently CBCT alone cannot be used for personalized dosimetry. Further studies should be done to investigate whether density differences at the voxel level in the perfused volume between tumor and non-tumoral liver could be used to calculate a T/N using only CBCT.

In conclusion, CBCT may be a reliable segmentation method, but it does not significantly increase the accuracy of dose prediction compared with that of  $^{99\text{m}}\text{Tc}$ -MAA SPECT/CT. At higher doses both methods tend to overestimate the doses to tumors and perfused livers. CBCT may be a useful segmentation method for complex cases if it is difficult to delineate perfused volumes in  $^{99\text{m}}\text{Tc}$ -MAA SPECT/CT images and may be particularly appropriate for radiation segmentectomy or for multiple injection sites.

## **Human rights**

The authors declare that the work described has been carried out in accordance with the Declaration of Helsinki of the World Medical Association revised in 2013 for experiments involving humans.

## **Informed consent and patient details**

The authors declare that this report does not contain any personal information that could lead to the identification of the patients. The authors declare that they obtained a written informed consent from the patients included in the article. The authors also confirm that the personal details of the patients have been removed.

## **Disclosure of interest**

The authors declare that they have no competing interest.

## **Funding**

This work did not receive specific funding.

## **Author contributions**

All authors attest that they meet the current International Committee of Medical Journal Editors (ICMJE) criteria for Authorship.

## References

- [1] Salem R, Padia SA, Lam M, Bell J, Chiesa C, Fowers K, et al. Clinical and dosimetric considerations for Y90: recommendations from an international multidisciplinary working group. *Eur J Nucl Med Mol Imaging* 2019;46:1695–704.
- [2] Kafrouni M, Allimant C, Fourcade M, Vauclin S, Guiu B, Mariano-Goulart D, et al. Analysis of differences between 99mTc-MAA SPECT- and 90Y-microsphere PET-based dosimetry for hepatocellular carcinoma selective internal radiation therapy. *EJNMMI Res* 2019;9:62.
- [3] Jadoul A, Bernard C, Lovinfosse P, Gérard L, Lilet H, Cornet O, et al. Comparative dosimetry between 99mTc-MAA SPECT/CT and 90Y PET/CT in primary and metastatic liver tumors. *Eur J Nucl Med Mol Imaging* 2020;47:828–37.
- [4] Garin E, Tselikas L, Guiu B, Chalaye J, Edeline J, De Baere T, et al. Major impact of personalized dosimetry using 90Y loaded glass microspheres SIRT in HCC: final overall survival analysis of a multicenter randomized phase II study (DOSISPHERE-01). *J Clin Oncol* 2020;38:S516.
- [5] Garin E, Lenoir L, Rolland Y, Laffont S, Pracht M, Mesbah H, et al. Effectiveness of quantitative MAA SPECT/CT for the definition of vascularized hepatic volume and dosimetric approach: phantom validation and clinical preliminary results in patients with complex hepatic vascularization treated with yttrium-90-labeled microspheres. *Nucl Med Commun* 2011;32:1245–55.
- [6] Kao YH, Hock Tan AE, Burgmans MC, Irani FG, Khoo LS, Gong Lo RH, et al. Image-guided personalized predictive dosimetry by artery-specific SPECT/CT partition modeling for safe and effective 90Y radioembolization. *J Nucl Med* 2012;53:559–66.
- [7] Bapst B, Lagadec M, Breguet R, Vilgrain V, Ronot M. Cone beam computed tomography (CBCT) in the field of interventional oncology of the liver. *Cardiovasc Intervent Radiol* 2016;39:8–20.
- [8] Louie JD, Kothary N, Kuo WT, Hwang GL, Hofmann LV, Goris ML, et al. Incorporating cone-beam CT into the treatment planning for yttrium-90 radioembolization. *J Vasc Interv Radiol* 2009;20:606–13.
- [9] van den Hoven AF, Prince JF, de Keizer B, Vonken E-JPA, Bruijnen RCG, Verkooijen HM, et al. Use of c-arm cone beam CT during hepatic radioembolization: Protocol optimization for extrahepatic shunting and parenchymal enhancement. *Cardiovasc Intervent Radiol* 2016;39:64–73.
- [10] O'Connor PJ, Pasik SD, van der Bom IM, Bishay V, Radaelli A, Kim E. Feasibility of yttrium-90 radioembolization dose calculation utilizing intra-procedural open trajectory cone beam CT. *Cardiovasc Intervent Radiol* 2020;43:295–301.

- [11] Ertreo M, Choi H, Field D, Lischalk JW, Cohen E, Lynskey GE, et al. Comparison of cone-beam tomography and cross-sectional imaging for volumetric and dosimetric calculations in resin yttrium-90 radioembolization. *Cardiovasc Intervent Radiol* 2018;41:1857–66.
- [12] Jafargholi Rangraz E, Coudyzer W, Maleux G, Baete K, Deroose CM, Nuyts J. Multi-modal image analysis for semi-automatic segmentation of the total liver and liver arterial perfusion territories for radioembolization. *EJNMMI Res* 2019;9:19.
- [13] Salem R, Lewandowski RJ, Gates VL, Nutting CW, Murthy R, Rose SC, et al. Research reporting standards for radioembolization of hepatic malignancies. *J Vasc Interv Radiol* 2011;22:265–78.
- [14] Dezarn WA, Cessna JT, DeWerd LA, Feng W, Gates VL, Halama J, et al. Recommendations of the American Association of Physicists in Medicine on dosimetry, imaging, and quality assurance procedures for 90Y microsphere brachytherapy in the treatment of hepatic malignancies. *Med Phys* 2011;38:4824–45.
- [15] Venkatanarasimha N, Gogna A, Tong KTA, Damodharan K, Chow PKH, Lo RHG, et al. Radioembolisation of hepatocellular carcinoma: a primer. *Clinical Radiology* 2017;72:1002–13.
- [16] Kim SP, Cohalan C, Kopek N, Enger SA. A guide to 90Y radioembolization and its dosimetry. *Med Phys* 2019;68:132–45.
- [17] Cui Z, Shukla PA, Habibollahi P, Park HS, Fischman A, Kolber MK. A systematic review of automated feeder detection software for locoregional treatment of hepatic tumors. *Diagn Interv Imaging* 2020;101:439–49.
- [18] TheraSphere yttrium-90 glass microspheres instructions for use 990252.SPE Rev. 8.3 biocompatibles UK limited - now part of the boston scientific group, surrey, GU9 8QL, United Kingdom. <https://www.bostonscientific.com/en-US/products/cancer-therapies/therasphere-y90-glass-microspheres.html> (accessed 15.04.20).
- [19] Lin LI-K. A concordance correlation coefficient to evaluate reproducibility. *Biometrics* 1989;45:255.
- [20] Partik B, Stadler A, Schamp S, Koller A, Voracek M, Heinz-Peer G, et al. 3D versus 2D ultrasound: accuracy of volume measurement in human cadaver kidneys. *Invest Radiol* 2002;37:489–95.
- [21] Bland JM, Altman DG. Statistical methods for assessing agreement between two methods of clinical measurement. *Int J Nurs Stud* 2010;47:931–6.
- [22] Passing H, Bablok W. A new biometrical procedure for testing the equality of measurements from two different analytical methods. Application of linear regression procedures for method comparison studies in clinical chemistry, Part I. *Clin Chem Lab Med* 1983;21.



- [23] Bilic-Zulle L. Comparison of methods: Passing and Bablok regression. *Biochem Med* 2011;49–52. h
- [24] Delicque J, Hermida M, Piron L, Allimant C, Belgour A, Pageaux G-P, et al. Intra arterial treatment of hepatocellular carcinoma: Comparison of MELD score variations between radio-embolization and chemo-embolization. *Diagn Interv Imaging* 2019;100:689–97.
- [25] Tong AKT, Kao YH, Too CW, Chin KFW, Ng DCE, Chow PKH. Yttrium-90 hepatic radioembolization: clinical review and current techniques in interventional radiology and personalized dosimetry. *Br J Radiol* 2016;89:20150943.
- [26] Palard X, Edeline J, Rolland Y, Le Sourd S, Pracht M, Laffont S, et al. Dosimetric parameters predicting contralateral liver hypertrophy after unilobar radioembolization of hepatocellular carcinoma. *Eur J Nucl Med Mol Imaging* 2018;45:392–401.
- [27] Garin E, Rolland Y, Laffont S, Edeline J. Clinical impact of 99mTc-MAA SPECT/CT-based dosimetry in the radioembolization of liver malignancies with 90Y-loaded microspheres. *Eur J Nucl Med Mol Imaging* 2016;43:559–75.
- [28] Gabr A, Ali R, Al Asadi A, Mora R, Mouli S, Riaz A, et al. Technical aspects and practical approach toward same-day Y90 radioembolization in the management of hepatocellular carcinoma. *Tech Vasc Interv Radiol* 2019;22:93–9.
- [29] Garin E, Rolland Y, Edeline J. 90Y-loaded microsphere SIRT of HCC patients with portal vein thrombosis: high clinical impact of 99mTc-MAA SPECT/CT-based dosimetry. *Semin Nucl Med* 2019;49:218–26.
- [30] Ray CE, Gaba RC, Knuttinen M-G, Minocha J, Bui JT. Multiple arteries supplying a single tumor vascular distribution: microsphere administration options for the interventional radiologist performing radioembolization. *Semin Intervent Radiol* 2014;31:203–6.
- [31] Kao Y-H, Steinberg JD, Tay Y-S, Lim GK, Yan J, Townsend DW, et al. Post-radioembolization yttrium-90 PET/CT - part 1: diagnostic reporting. *EJNMMI Res* 2013;3:56.
- [32] Elschot M, Vermolen BJ, Lam MGEH, de Keizer B, van den Bosch MAAJ, de Jong HWAM. Quantitative comparison of PET and bremsstrahlung SPECT for imaging the in vivo yttrium-90 microsphere distribution after liver radioembolization. *PLoS One* 2013;8:e55742.
- [33] Minarik D, Sjögreen Gleisner K, Ljungberg M. Evaluation of quantitative <sup>90</sup>Y SPECT based on experimental phantom studies. *Phys Med Biol* 2008;53:5689–703.
- [34] Roshan HR, Azarm A, Mahmoudian B, Islamian JP. Advances in SPECT for optimizing the liver tumors radioembolization using yttrium-90 microspheres. *World J Nucl Med* 2015;14:75–80.

## Figure Legends

**Figure 1.** Flow chart diagram of patient selection.

**Figure 2.** Eighty-two-year-old woman with an infiltrative hepatocellular carcinoma of the right liver (procedure number 11). Figures show the perfused volume segmentation from cone-beam CT (CBCT) (A) with manually defined contours and from  $^{99m}\text{Tc}$ -MAA SPECT/CT (B) with semi-automatically method based on thresholding. Dosimetry data: 171.8 Gy for  $D_{\text{PL}}$ -CBCT and 190.2 Gy for  $D_{\text{PL}}$ - $^{99m}\text{Tc}$ -MAA SPECT/CT.

**Figure 3.** Boxplots in the figure show the mean doses (Gy) absorbed by tumors ( $D_{\text{T}}$ ) (A) and non-tumoral livers ( $D_{\text{NTL}}$ ) (B), as calculated using cone-beam CT (CBCT),  $^{99m}\text{Tc}$ -MAA SPECT/CT, and  $^{90}\text{Y}$  imaging.

**Figure 4.** Modified Bland-Altman analysis of all 17 post- versus pre-treatment mean tumor doses ( $D_{\text{T}}$ ; A and C) and non-tumoral liver doses ( $D_{\text{NTL}}$ ; B and D) derived using cone-beam CT (CBCT) (top) and  $^{99m}\text{Tc}$ -MAA SPECT/CT (bottom). The median (1<sup>st</sup> to 3<sup>rd</sup> quartile) differences between the post- and pre-treatment dosimetry data are shown. The  $D_{\text{T}}$  variations were markedly higher for tumors exhibiting greater uptake.

**Figure 5.** Passing–Bablok graphical representations of the regression lines for the mean tumor doses ( $D_{\text{T}}$ ) (A and C) and perfused livers ( $D_{\text{PL}}$ ) (B and D), as calculated using cone-beam CT (CBCT) (top) and  $^{99m}\text{Tc}$ -MAA SPECT/CT (bottom), compared with the  $^{90}\text{Y}$  imaging data. The regression equations ( $y = a + bx$ ) with 95% confidence intervals for slope are shown for each graph.

**Figure 6.** Seventy-one-year-old man with an infiltrative hepatocellular carcinoma of the left liver (procedure number 3). Figures show that the perfused volume from cone-beam CT (CBCT) (A) better correlated than the  $^{99m}\text{Tc}$ -MAA SPECT/CT data (B) with the perfused volume from  $^{90}\text{Y}$  SPECT/CT (C). Dosimetry data: 233.9 Gy for  $D_{\text{PL}}$ -CBCT, 271.3 Gy for  $D_{\text{PL}}$ - $^{99m}\text{Tc}$ -MAA SPECT/CT and 244.8 Gy for  $D_{\text{PL}}$ - $^{90}\text{Y}$  imaging.

**Table 1.** Procedures characteristics.

**Table 2.** Differences between the delivered and planned doses as revealed by  $^{90}\text{Y}$  imaging and either CBCT or  $^{99m}\text{Tc}$ -MAA SPECT/CT (Gy).

**Table 3.** Mean values of the absorbed doses (Gy) using the three dosimetric evaluations performed for each procedure.

**Table 4.** Lin's concordance coefficient correlations ( $\rho$  values) of the mean absorbed doses and perfused volumes.

20 patients with HCC who underwent radioembolization with glass microspheres assessed for eligibility between December 2014 and June 2019

Excluded patients (n = 5)

Different injection site between work-up and treatment day (n = 1)

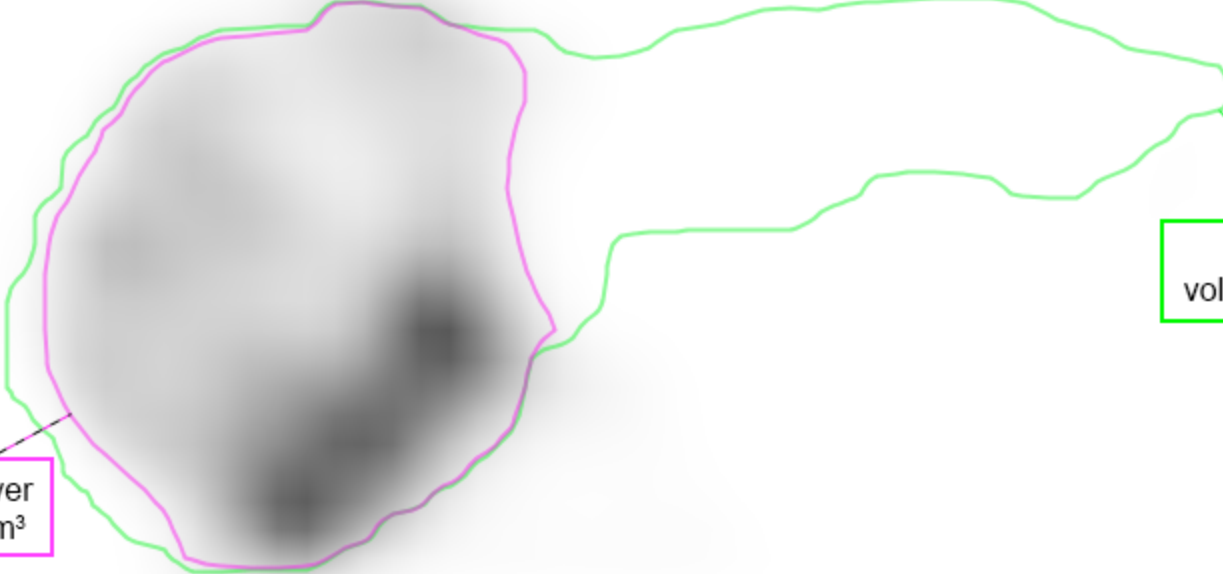
Multiple injection sites (n = 3)

Poor image quality (n = 1)

15 patients (with 17 procedures)  
ultimately included in the study



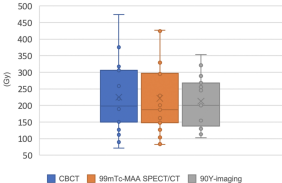
CBCT perfused liver  
volume 426.8 cm<sup>3</sup>



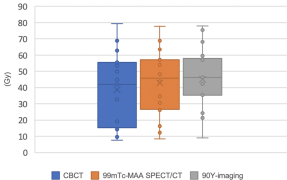
MAA perfused liver  
volume 448.4 cm<sup>3</sup>

Whole liver  
volume 1002.6 cm<sup>3</sup>

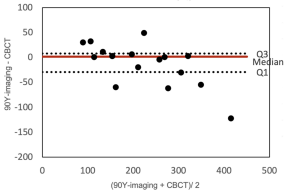
Tumor mean dose ( $D_T$ )



Non-tumoral liver mean dose ( $D_{NTL}$ )

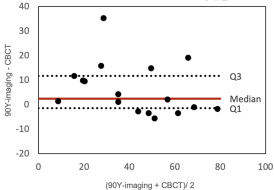


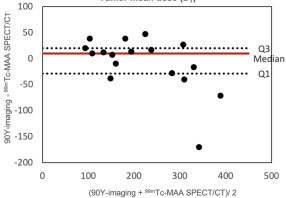
Tumor mean dose ( $D_T$ )



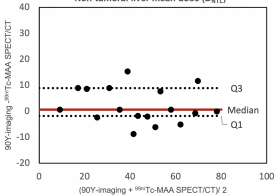


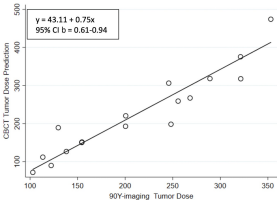
Non-tumoral liver mean dose ( $D_{NTL}$ )

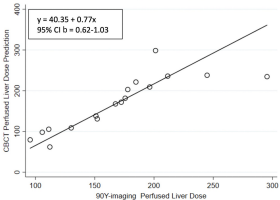


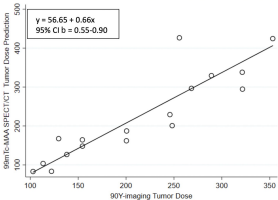
Tumor mean dose ( $D_T$ )

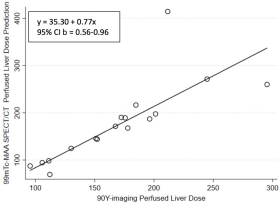
Non-tumoral liver mean dose ( $D_{HTL}$ )

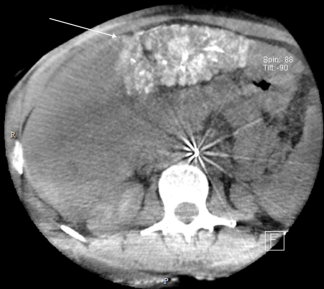




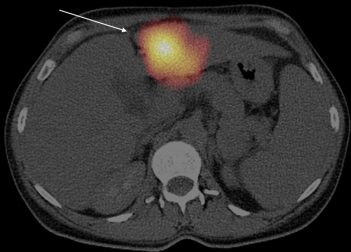


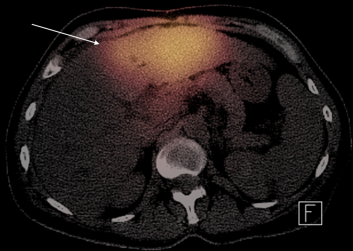












Characteristics	Value
No. of procedures	17 (17/17; 100%)
No. of patients	15 (15/15; 100%)
Age (years)	68.3 ± 10.5 [47–82]
Sex (n)	
Male	8 (8/15; 53%)
Female	7 (7/15; 47%)
Hepatic function	
No cirrhosis	2 (2/17; 12%)
Child–Pugh A5	7 (7/17; 41%)
Child–Pugh A6	7 (7/17; 41%)
Child–Pugh B7	1 (1/17; 6%)
ECOG status	
0	11 (11/17; 65%)
1	5 (5/17; 29%)
2	1 (1/17; 6%)
BCLC stage	
B	1 (1/17; 6%)
C	16 (16/17; 94%)
MELD score	8.7 ± 1.8 [6–12]
Prior local therapy *	
Yes	7 (7/17; 41%)
No	10 (10/17; 59%)
HCC diagnosis	
Biopsy proven	3 (3/17; 18%)
Typical imaging features	14 (14/17; 82%)
Multifocal disease	
Yes	11 (11/17; 65%)
No	6 (6/17; 35%)
Tumor morphology	
Infiltrative	15 (15/17; 88%)
Nodular	2 (2/17; 12%)
Tumor volume (cm <sup>3</sup> )	364.3 ± 272.7 [19.8–841.4]
Portal vein invasion	
Yes	15 (15/17; 88%)
No	2 (2/17; 12%)
Treatment	
Hemiliver	12 (12/17; 71%)
Sectorial	4 (4/17; 23%)
Segmental	1 (1/17; 6%)
Lung shunt fraction (%)	
Median	2
(Q1; Q3)	(1.3; 3) [1–10]

ECOG: Eastern Cooperative Oncology Group; HCC: hepatocellular carcinoma; MELD: Model for End-stage Liver Disease; Q: quartile.

Qualitative variables are expressed as raw numbers, numbers in parentheses as proportions followed by percentages.

If normally distributed, quantitative variables are expressed as means ± standard deviation; numbers in brackets are ranges.

If not normally distributed, quantitative variables are expressed as medians (Q1; Q3).

\*Prior local therapies included chemoembolisation and radiofrequency ablation.

<sup>90</sup> Y imaging - CBCT					<sup>90</sup> Y imaging - <sup>99m</sup> Tc-MAA SPECT/CT			
	D <sub>PL</sub>	D <sub>T</sub>	D <sub>PNTL</sub>	D <sub>NTL</sub>	D <sub>PL</sub>	D <sub>T</sub>	D <sub>PNTL</sub>	D <sub>NTL</sub>
Median	5.8	1.6	26.5	2.5	5.6	9.8	4.8	0.6
Q1	-12.7	-29	-4.6	-1.5	-13.6	-28.4	-20	-1.86
Q3	16.1	7.53	51.4	11.7	10.2	19.9	39.6	8.9

Mean absorbed doses (Gy) by the perfused liver (D<sub>PL</sub>), tumor (D<sub>T</sub>), perfused non-tumoral liver (D<sub>PNTL</sub>), and non-tumoral liver (D<sub>NTL</sub>).

Procedure	CBCT		<sup>99m</sup> Tc-MAA SPECT/CT				<sup>90</sup> Y imaging					
	D <sub>PL</sub>	D <sub>T</sub>	D <sub>PNTL</sub>	D <sub>NTL</sub>	D <sub>PL</sub>	D <sub>T</sub>	D <sub>PNTL</sub>	D <sub>NTL</sub>	D <sub>PL</sub>	D <sub>T</sub>	D <sub>PNTL</sub>	D <sub>NTL</sub>
1	61.9	89.9	47.3	7.5	69.3	83.5	59.9	8.5	112.1	122.1	102.9	9
2	235.8	259	111.7	19.1	414.4	426.5	256.5	26.2	211.6	255.7	184.5	35.4
3	237.9	267.2	134.6	56.2	271.3	296.7	172.8	63.5	244.8	268.2	186.1	75.4
4	202.9	192.8	203.7	68.9	167.6	161.9	167.9	68.8	177.9	200.4	176.3	68.1
5	167.6	150.3	174.8	79.4	171.4	164.3	173.7	77.7	167.5	154.4	170.2	77.9
6	108.7	126.6	76.8	32.7	124.6	126.7	123.4	45.8	130.1	138.1	103.3	37
7	137.9	151.5	25.1	10.9	145.4	148.2	71	30.7	151	154.5	121.3	46.3
8	130.8	474.1	120.5	34.2	144	424.4	134.1	34.6	152.1	353.2	145.1	35.4
9	98.1	111.8	34.1	9.6	94.3	103.6	41.7	12.2	105.7	113.4	81.8	21.3
10	105.4	189.2	53.6	15.3	98.4	167.4	53.3	16.3	111.2	129.6	92.9	25.2
11	171.8	318.2	130.9	55.5	190.2	329.3	149	57.1	172.4	289.1	136.9	58
12	221.3	317.7	191.7	62.8	216.4	294.6	192.4	64.4	184.7	321.5	151.5	59.6
13	209.1	220.4	96.4	14.3	186.9	187.2	158.8	26.7	196.4	200.6	135.3	24.3
14	234.5	375.5	162	41.9	260	338	212	49.2	295.4	321.3	279	57.1
15	181.6	198.3	177.4	53.5	189.3	200.8	186.4	54	175.7	248.1	153.2	48
16	79.4	71.7	82.2	44.8	87.3	83	88.3	43.9	95.5	102.9	93.2	42.3
17	298.5	306.2	195.6	49.8	197.5	229.2	132.8	48.2	201.3	245.8	132.2	46.3

Mean absorbed doses (Gy) by the perfused liver (D<sub>PL</sub>), tumor (D<sub>T</sub>), perfused non-tumoral liver (D<sub>PNTL</sub>), and non-tumoral liver (D<sub>NTL</sub>).

Mean absorbed dose (Gy)													Perfused volume (cm <sup>3</sup> )		
Modality	CBCT				<sup>99m</sup> Tc-MAA SPECT/CT				<sup>90</sup> Y imaging				CBC	<sup>99m</sup> Tc-MAA SPECT/CT	<sup>90</sup> Y imaging
	D <sub>P</sub>	D <sub>T</sub>	D <sub>PN</sub>	D <sub>N</sub>	D <sub>P</sub>	D <sub>T</sub>	D <sub>PN</sub>	D <sub>N</sub>	D <sub>P</sub>	D <sub>T</sub>	D <sub>PN</sub>	D <sub>N</sub>	V <sub>PL</sub>	V <sub>PL</sub>	V <sub>PL</sub>
	L		TL	TL	L		TL	TL	L		TL	TL			
Intraobserver reliability	0.99	0.98	0.98	0.99	0.97	0.97	0.94	0.99	0.94	0.99	0.90	0.98	0.99	0.96	0.96
Interobserver reliability	0.96	0.97	0.84	0.96	0.96	0.95	0.80	0.95	0.82	0.91	0.85	0.98	0.98	0.89	0.97

Mean absorbed doses (Gy) by the perfused liver (D<sub>PL</sub>), tumor (D<sub>T</sub>), perfused non-tumoral liver (D<sub>PNTL</sub>), and non-tumoral liver (D<sub>NTL</sub>). V<sub>PL</sub>: mean perfused volume (cm<sup>3</sup>).